Progress In Electromagnetics Research C, Vol. 173, 299–307, 2026

PIER C

(Received 22 July 2026, Accepted 11 September 2026, Scheduled 20 September 2026)

Vibration Analysis and Optimization of Flux Reversal PM Machine with PM Chamfer

Bo Tian[1], Qiang Shi[1], Jianyi Yang[1], Guofeng Diao[1], Mingxin Luo[1], and Libing Jing[2,*]

[1]Liujiaxia Hydropower Plant, State Grid Gansu Electric Power Company, Linxia 731699, China
[2]College of Electrical Engineering and New Energy, Hubei Provincial Engineering Technology Research Center for Microgrid
China Three Gorges University, Yichang 443002, China

ABSTRACT: Flux reversal permanent magnet machine (FRPMM), owing to its high power density and excellent low-speed high-torque capability, is considered promising for low-speed direct-drive hydropower generation systems. However, the vibration and noise caused by radial electromagnetic force hinder the development of the FRPMM. A novel FRPMM with a permanent magnet (PM) chamfer on the stator is proposed. First, the radial force density, average torque, and torque ripple are taken as optimization objectives. The multi-objective genetic algorithm (MOGA) is used to optimize the machine. Next, the space-time characteristics of air-gap flux density and radial force density are obtained based on finite-element simulation. The modal analysis and harmonic response analysis of the stator are carried out. The results show that the radial force density of the proposed FRPMM is significantly reduced, and the machine's vibration characteristics are optimized.

1. INTRODUCTION

Pumped-storage, conventional small hydropower systems are evolving toward low-speed direct-drive, high-efficiency, and highly reliable operation. Flux reversal permanent magnet machine (FRPMM), featuring high power density, have attracted increasing attention in hydropower generator applications [1, 2]. However, during operation, electromagnetic vibration and noise limit FRPMM applicability in precision-oriented applications [3]. Due to the doubly salient structure and high air-gap flux density, the FRPMM exhibits significant cogging torque, which is the primary cause of torque ripple, inducing electromagnetic vibration and acoustic noise [4].

Vibrations are primarily attributed to mechanical sources, aerodynamic noise, and electromagnetic excitation forces [5]. Periodic deformation of the stator is induced by radial electromagnetic force waves, which are identified as the dominant mechanism of electromagnetic vibration [6]. In topology optimization, stator tooth-shape modifications have been proven to reduce low-order electromagnetic force harmonics. Radial force wave amplitudes in high-torque-density machines are reduced using single/double-slot correction techniques [7]. Similarly, a parabolic stator tooth-tip optimization is proposed in [8], which suppresses first-order slot harmonic vibration and reduces vibration acceleration. Comparative studies on stator chamfer types have shown that rounded chamfers maximize cogging-effect reduction. Linear chamfers have been demonstrated to effectively suppress load torque ripple [9]. Rotor structure innovations are also considered critical. Torque ripple is reduced by staggered segmented rotors through phase-cancellation principles [10]. A skewed pole segmentation model for fractional-slot machines is developed in [11], where multi-order noise is attenuated via axial modal decoupling. Additionally, asymmetric rotor and segmented rotor designs are proposed to mitigate radial electromagnetic forces, providing new insights into vibration suppression [12, 13]. Although these existing techniques have contributed to vibration suppression to varying degrees, they generally compromise output torque, thereby limiting overall performance. In addition, with PMs mounted on the stator, geometric modifications of the PMs in the FRPMM offer an additional degree of freedom to suppress vibrations [14]. However, this approach has received little attention in FRPMM vibration studies.

Electromagnetic force harmonic analysis is the theoretical basis for vibration optimization. Systematic summary of the spatiotemporal modulation effects of electromagnetic force waves in [15] reveals that coupling between stator slots and rotor pole geometry introduces higher-order harmonic components. Furthermore, the frequency-shift phenomenon reported in [16] demonstrates that balanced branch currents suppress vibrations at specific frequencies. In [17], the magnetostrictive effects of high-silicon steel and amorphous alloys are quantitatively compared to guide magnetic material selection. The injection of the field winding harmonic current successfully compensates for the 0-order radial modal vibration in [18].

Regarding optimization methods, single-objective optimization focuses solely on cogging torque reduction, resulting in performance degradation in other aspects [19]. The analytical model proposed in [20] is insufficient for accurately describing the force wave modulation effects in complex topologies. Conventional genetic algorithms suffer from slow convergence and suboptimal solution sets in multiparameter optimization [21]. Differential evolution has been applied to optimize

* Corresponding author: Libing Jing (jinglibing163@163.com).

poleslot combinations for reducing unbalanced magnetic forces [22]. Yet its potential for vibration characteristic optimization remains unexplored.

Unlike conventional designs focusing on cogging torque and torque ripple reduction, this study proposes a PM chamfer design for a 12-slot/17-pole FRPMM to synergistically improve torque and mitigate vibration, where torque average, torque ripple, and dominant electromagnetic force harmonics are simultaneously optimized via the multi-objective genetic algorithm (MOGA). The air-gap flux density distribution is solved using the Maxwell electromagnetic field analysis tool. The Spatiotemporal characteristics are analyzed through Fourier decomposition methods. Natural frequencies and mode shapes are obtained by combining stator modal frequency characteristics testing. The vibration suppression effect of topology improvement is verified through electromagnetic-mechanical coupling simulations. Section 2 describes the machine topology and operational principles. In Section 3, the machine is optimized to maximize average torque while minimizing torque ripple and radial electromagnetic force. Section 4 compares and analyzes the machine's electromagnetic fields. Section 5 presents the stator harmonic response and modal analysis coupling analysis. Section 6 summarizes research findings.

2. TOPOLOGY AND WORKING PRINCIPLE

2.1. Topology

Fig. 1 shows the structure of the proposed FRPMM. A combination of alternating poles and auxiliary teeth is adopted. In addition, an arc-shaped protrusion near the air-gap side is used in the permanent magnet (PM) on the stator. The air-gap reluctance distribution is adjusted. Magnetic leakage is minimized, and the machine's electromagnetic performance is optimized. Table 1 lists the machine's key parameters.

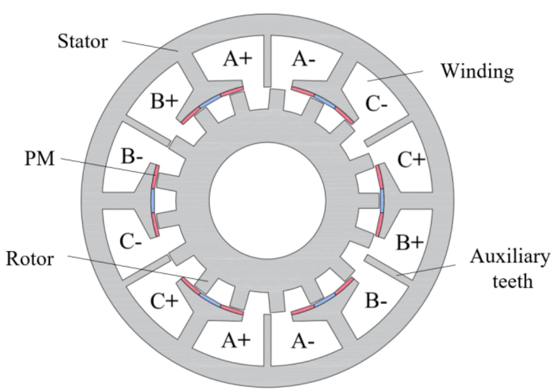

FIGURE 1. Topology of the proposed FRPMM.

2.2. Principle of Operation

The main magnetic flux is directed radially from PMs into the air gap. Radial forces are generated on the stator tooth surfaces, leading to electromagnetic noise and vibrations. The radial electromagnetic force F_r acting on the inner surface of the stator core is determined by the air-gap magnetic field, which

TABLE 1. Main parameters of the FRPMM.

Parameters	Value
Axial length (mm)	60
Outer radius of machine (mm)	6
Number of poles	17
Number of slots	12
Rated speed (r/min)	1000
Supplied current (A)	10
Series turns per phase	30
PM material	NdFeB
Iron material	DW315-50

can be expressed as:

$$F_r = \frac{1}{2\mu_0}\left[B_r^2 - B_t^2\right] \tag{1}$$

where B_r and B_t are the radial and tangential components of the air-gap flux density, respectively, and μ_0 is the vacuum permeability. The tangential component is generally much smaller than that of the radial component. Thus, the equation can be simplified as:

$$F_r \approx \frac{1}{2\mu_0} B_r^2 \tag{2}$$

The radial flux density B_r in the machine air gap is determined by the product of the air-gap magnetomotive force (MMF) f and air-gap permeance Λ. The mathematical expression for B_r is given as:

$$\begin{aligned} B_r &= f \cdot \Lambda = (f_r + f_s) \cdot \Lambda \\ &= \left[\sum_{\mu} F_\mu \cos(\mu\omega t - \mu p\theta) + \sum_{\nu} F_\nu \cos(\omega t \pm \upsilon p\theta)\right] \cdot \Lambda \end{aligned} \tag{3}$$

where F_μ is the μ-th harmonic amplitude of the PM MMF; μ is specified as an odd sequence ($\mu = 1, 3, 5\ldots$); F_ν is expressed as the ν-th harmonic amplitude of the stator MMF ($\nu = (6k+1)\cdot p$, $k \in N^+$); p represents the number of pole pairs; ω denotes the rotor angular velocity; θ is defined as the circumferential angle of the air gap.

Under idealized conditions where rotor eccentricity is neglected, and the rotor surface is assumed to be smooth, the air-gap permeance comprises a constant component and a periodically modulated component induced by stator slotting:

$$\Lambda = \Lambda_0 + \sum \Lambda_k \cos(kN_{ss}\theta) \tag{4}$$

where Λ_0 is the constant permeability of the air gap; Λ_k is the air gap permeability caused by the stator slot; N_{ss} is the number of stator slots.

The spatiotemporal distribution of the radial electromagnetic force is derived by synthesizing Eqs. (2)–(4). The derived expression is formulated as follows:

$$F_r = \sum_r p_r \cos(\omega_r t - r\theta + \varphi_r) \tag{5}$$

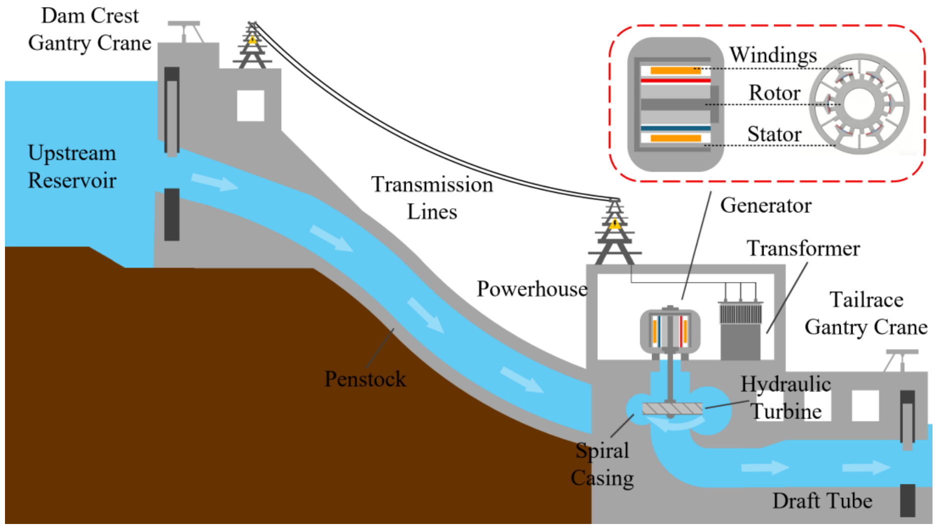

FIGURE 2. Configuration of the proposed FRPMM-based hydropower generation unit.

where r is the spatial order of the electromagnetic force wave ($r = \mu \pm \nu$); ω_r is the rotation angular velocity of r-th electromagnetic force wave; p_r is the amplitude of r-th force wave; φ_r is the phase angle.

The vibration response of machines is primarily excited by low-order spatial harmonic excitations that act on the stator. The conversion efficiency of energy from electromagnetic excitation to mechanical vibration is enhanced when the spatial order of the radial force is reduced. For fractional-slot winding configurations, the dominant spatial force wave components are predominantly distributed in the low-order regions due to their harmonic-order characteristics. Consequently, significant structural vibrations are likely induced in the system.

2.3. Hydroelectric Power Generation System

Figure 2 illustrates the application of the proposed FRPMM in a low-speed direct-drive hydropower generation unit. The hydropower generation system mainly consists of a hydraulic turbine, coupling, FRPMM, transformer, and utility grid. During operation, water flows through the spiral casing to drive the hydraulic turbine, and the generated mechanical power is directly transmitted to the FRPMM via the coupling. The three-phase alternating current generated by the FRPMM is regulated by a transformer and then delivered to the utility grid, enabling the efficient conversion of mechanical energy into electrical energy.

The FRPMM adopts a low-speed direct-drive configuration, eliminating the gearbox. This configuration reduces mechanical transmission losses, simplifies the drivetrain, and enhances overall system efficiency and reliability.

3. PARAMETER OPTIMIZATION DESIGN

3.1. Optimization Objectives and Variables

Geometric parameters of the proposed machine are related to electromagnetic field characteristics and coupled with electromechanical vibration characteristics. To achieve an optimal trade-off between electromagnetic performance and mechanical stability, a MOGA is employed for structural parameter optimization.

Before conducting multi-objective optimization, the relationship between optimization objectives and design variables must be established. This study focuses on the vibration suppression of FRPMM. The amplitude of electromagnetic forces and torque ripple is the primary cause of vibration. A higher amplitude of the electromagnetic forces results in an increased vibration amplitude. Torque ripple induces periodic rotational-speed variations in the rotor, which generates mechanical vibration. Therefore, the following three objectives are selected for optimization. Table 2 lists the machine's optimization objectives and constraints.

TABLE 2. Optimization objectives and constraints of FRPMM.

Optimization object	Constraints
Radial force density amplitude	Min
Average torque	Max
Torque ripple	Min

1) Minimization of electromagnetic force amplitude (F_r): the radial electromagnetic force amplitude is taken as the optimization objective to optimize the machine's vibration characteristics and improve its operational stability and comfort.

2) Maximizing the average output torque (T_{avg}): the average output torque is taken as the optimization objective to improve the machine's output capacity.

3) Minimization of torque ripple (T_{pkavg}): the torque ripple is taken as the optimization goal to ensure the stability of the machine's output torque during operation and then optimize its vibration characteristics.

As shown in Fig. 3, main optimization variables include PM thickness h_1 and width θ_2, stator pole shoe thickness h_2, rotor slot depth h_3 and width θ_1.

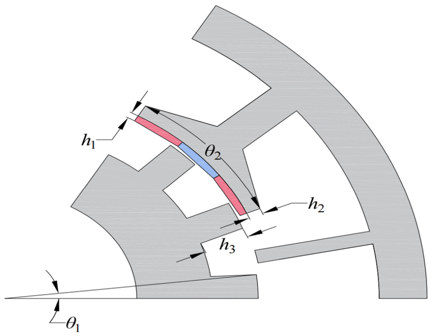

FIGURE 3. Structural parameters.

TABLE 3. Comparison of FRPMM optimization.

Parameter	Conv.	I	II	III
h_1	2.12	0.72	0.75	0.74
h_2	1.34	2.10	2.19	2.13
h_3	7.07	5.84	5.91	6.24
θ_1	6.12	8.02	8.04	8.04
θ_2	23.42	36.08	36.12	36.12
F_r/(N/m^2)	113061.97	68383.39	70112.89	69814.40
T_{avg}/(N · m)	2.87	3.68	3.67	3.67
T_{pkavg}/%	2.8	1.05	1.05	1.08

3.2. Optimization Design Process and Results

A genetic algorithm is applied to perform multi-objective optimization, and Fig. 4 presents the corresponding procedure. The desired values of the design variables are determined based on the extreme points and optimal value ranges. These values are subsequently validated. In the genetic algorithm optimization process, 5000 samples are initially generated. A total of 1000 samples are generated in each cycle. Three candidate samples are identified within a maximum of 20 iterations, as shown in Table 3. Due to the high requirements for the performance and vibration characteristics, candidate I is selected as the optimal solution by a comprehensive consideration of all optimization objectives.

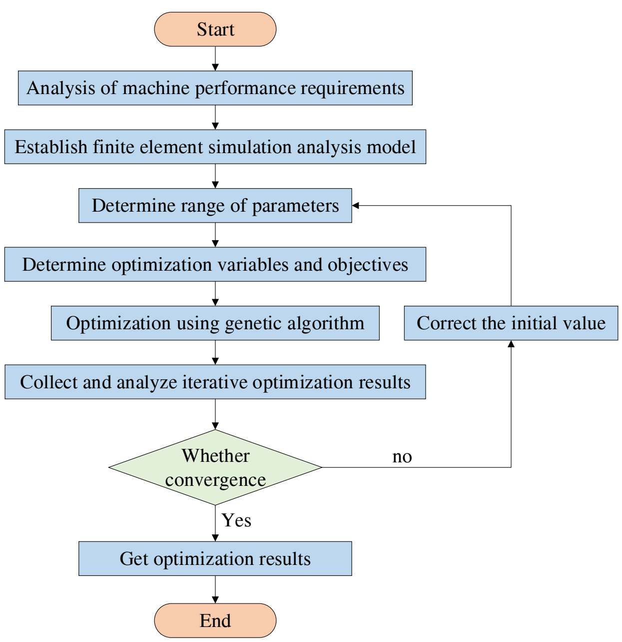

FIGURE 4. Optimization process of the proposed FRPMM.

4. ELECTROMAGNETIC PERFORMANCE

4.1. Flux Density

Since the radial component of the air-gap flux density is significantly larger than the tangential component, the radial flux density under no-load operation is analyzed and presented in Fig. 5. Fig. 5(a) shows the waveform comparison between the conventional and proposed machines, and the proposed machine shows a lower peak B_r amplitude. Fig. 5(b) further presents the corresponding harmonic spectra. The proposed machine shows reduced amplitudes in the low-order harmonic components, which is beneficial for vibration suppression. Furthermore, according to magnetic field modulation theory, the 18th and 24th harmonics dominate torque generation in the proposed machine, and the enhancement of these harmonic amplitudes contributes to improved output torque.

4.2. Radial Electromagnetic Force

Vibration is proportional to the amplitude of the radial electromagnetic force and inversely proportional to the fourth power of its spatial order. Therefore, priority is given to reducing radial electromagnetic forces with high amplitudes and low spatial orders, significantly suppressing machine vibration.

Fig. 6 shows spatiotemporal distributions of the radial electromagnetic forces. The proposed machine has a reduction of 57.25% in the ($0f$, 17), 84.89% in the ($0f$, 24), and 57.21% in the ($1f$, 5) compared to the conventional machine, and the radial electromagnetic force is reduced by 39.52%. These low-order spatial harmonics are the primary contributors to stator vibration due to strong coupling with low-order structural modes. Additionally, the force spectrum of the proposed machine shows broader spatial harmonic distribution, which helps distribute vibration energy across a wider frequency range and thus reduces the likelihood of resonance excitation.

4.3. Torque

Figure 7 compares the torque characteristics of conventional and proposed machines. The electromagnetic torque of 3.68 N · m is achieved by the proposed machine, demonstrating a 28.22% improvement over 2.87 N · m of the conventional machine. Additionally, the torque ripple is reduced from 2.80% to 1.05% in the proposed machine, with a reduction of 49.52%. Table 4 summarizes the key electromagnetic performance comparisons between the conventional and proposed machines. Benefiting from the alternate-pole configuration, the proposed machine shows enhanced output power and efficiency with reduced PM volume. Notably, as a flux-modulation machine, the proposed FRPMM achieves an improved power factor, yet it remains inherently lower than that of conventional PM synchronous machines [23].

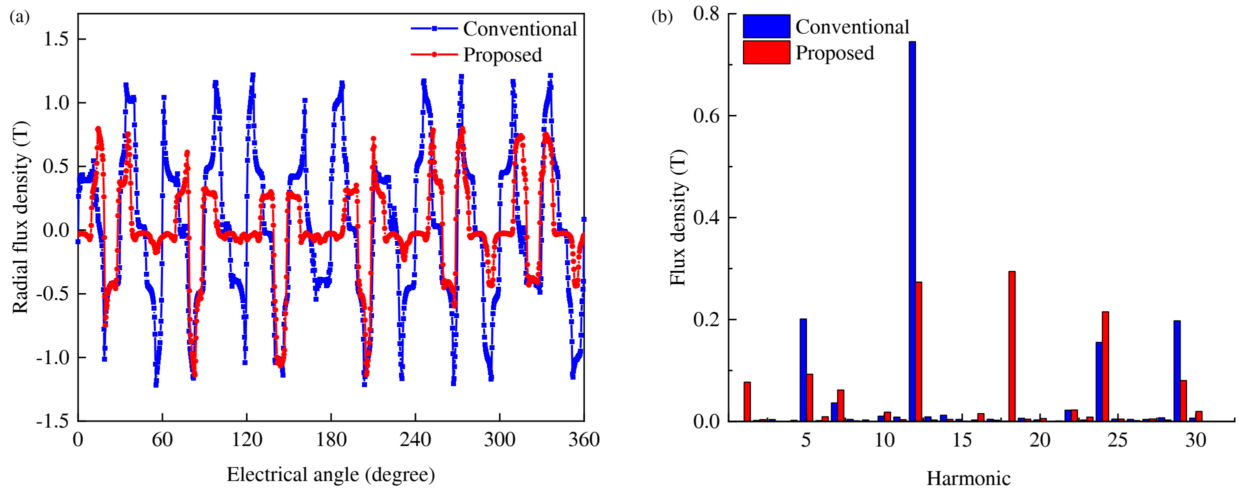

FIGURE 5. Radial air-gap flux density. (a) Air-gap flux density distribution and (b) harmonic spectra.

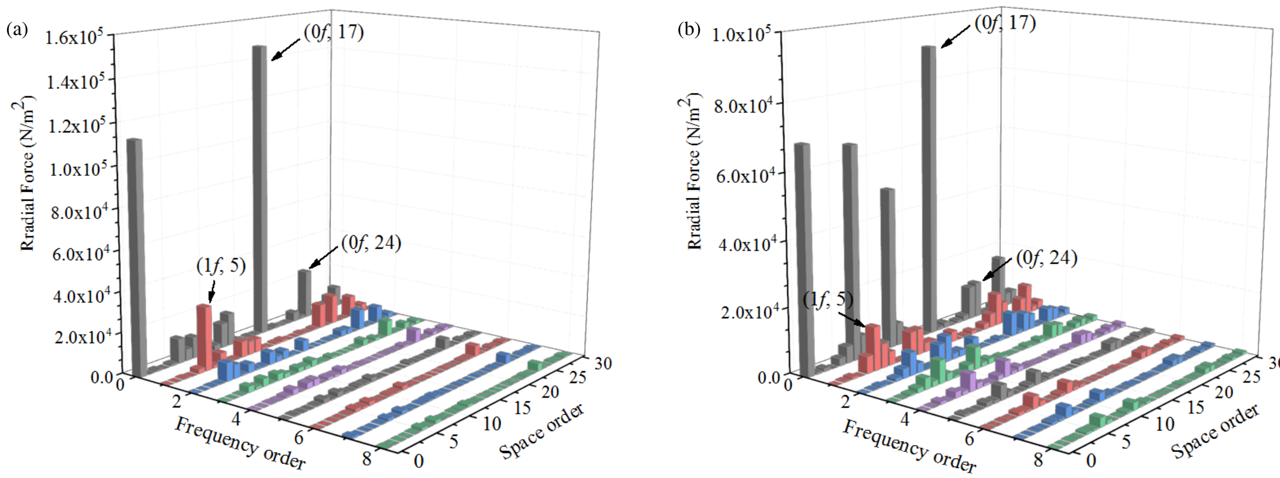

FIGURE 6. FFT-2D results of radial electromagnetic force. (a) Conventional machine. (b) Proposed machine.

TABLE 4. Key electromagnetic performance comparison.

Parameter	Conventional machine	Proposed machine
PM volume (m^3)	9.5×10^{-6}	6.4×10^{-6}
$T_{avg}/(N \cdot m)$	2.87	3.68
$T_{pkavg}/\%$	2.80%	1.05%
Output power (W)	300.5	385.4
Total loss (W)	36.8	39.0
Efficiency	89.1%	90.8%
Power factor	0.77	0.83

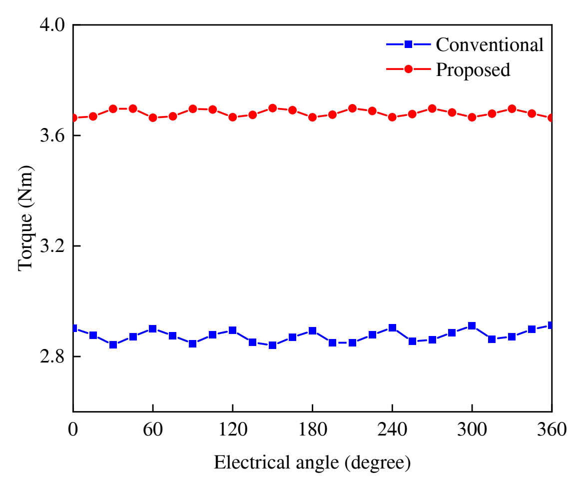

FIGURE 7. Torque characteristics.

5. MODAL AND VIBRATION ANALYSIS

5.1. Modal Analysis

The stator vibration is caused by radial electromagnetic forces. The vibration amplitude is jointly influenced by the spatial order and amplitude of the electromagnetic force waves and the natural frequency of the stator. When the stator is equivalently modeled as a cylindrical shell, the vibration displacement induced by the r-th order radial electromagnetic force can be expressed as:

$$A_m = \frac{F_m/M}{\sqrt{(\omega_m^2 - \omega_r^2)^2 + 4\zeta_m \omega_r^2 \omega_m^2}} \tag{6}$$

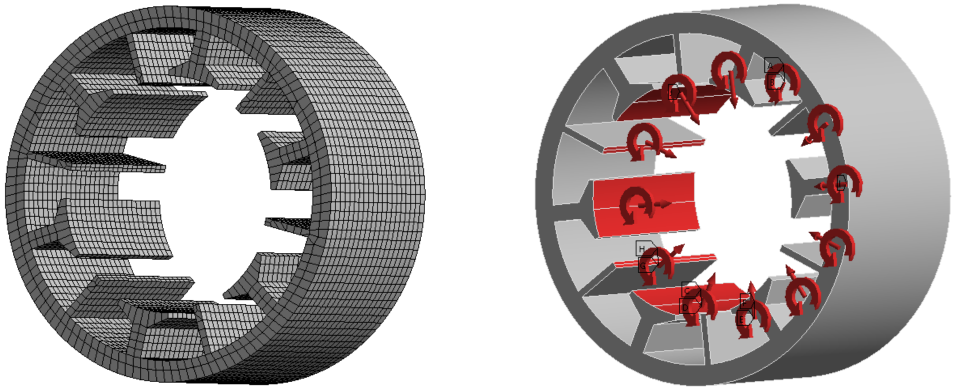

FIGURE 8. Stator mesh and electromagnetic force loading.

where M is the stator mass; ω_m is the m-th inherent angular frequency; and F_m can be expressed as:

$$F_m = \pi D L p_r \tag{7}$$

where D is the inner diameter of the core; L is the effective length of the machine core; and ζ_m is the modal damping ratio, expressed as:

$$\zeta_m = \frac{a f_m + b}{2\pi} = \frac{2.76 \times 10^{-5} f_m + 0.062}{2\pi} \tag{8}$$

where f_m denotes the m-th modal natural frequency; a is the mass-proportional damping coefficient; and b is the stiffness-proportional damping coefficient. The coefficients are determined based on the empirical damping characteristics of the stator core.

The stator's vibration displacement is proportional to the amplitude of radial force waves and inversely proportional to their spatial order. Resonance effects are produced in the system when the frequency of radial force waves approaches the stator's natural frequency. Based on this principle, the amplitudes of radial force waves with frequencies near the natural frequency are minimized. This strategy is critical for suppressing vibration. To avoid resonance phenomena, the stator's modal frequencies are calculated.

Finite-element simulations of the natural modes are performed for the stator core of the conventional machine. The stator's natural frequencies are analyzed. Finite-element simulations are also conducted for the proposed machine with identical material parameters. Table 5 lists comparative results of the modal simulations. The local structural stiffness of the stator core is enhanced by auxiliary teeth. The alternate-pole design effectively avoids asymmetric vibration modes and reduces the risk of multi-order modal coupling. As a result, the stator exhibits higher natural frequencies, improved system stiffness, and consequently better vibration suppression performance.

TABLE 5. Natural frequency of the stator.

Order	Conventional	Proposed	Variation
2	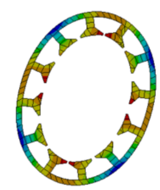 496.6 Hz	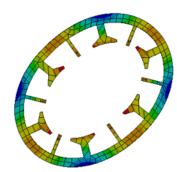 1059.8 Hz	113.41%
3	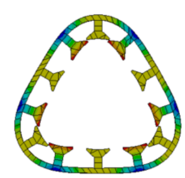 1323.0 Hz	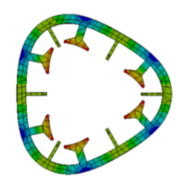 2732.5 Hz	106.54%
4	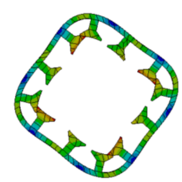 2351.0 Hz	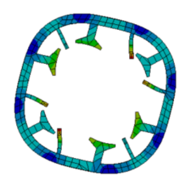 4716.8 Hz	100.63%
5	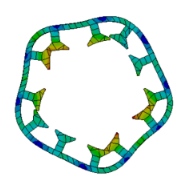 3404.0 Hz	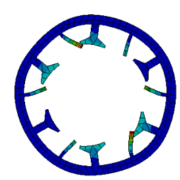 5846.1 Hz	71.74%

5.2. Vibration Analysis

Figure 8 illustrates the stator mesh and electromagnetic force-loading procedure. The stator is meshed with tetrahedral elements. The electromagnetic force density on each stator tooth element at each time step is extracted from transient finite element solutions and mapped onto the structural finite element model as nodal loads via interpolation. Combined with stator mode shapes, which naturally incorporate both global and local deformations, harmonic response analysis is then performed using the mode superposition method to obtain the stator's vibration deformation, velocity, and acceleration responses under various excitation frequencies.

The stator vibration displacement variation is obtained by finite-element analysis, as shown in Fig. 9. The displacement

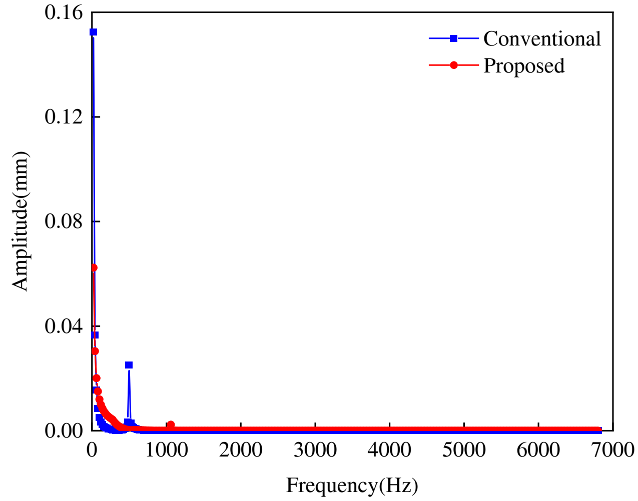

FIGURE 9. Vibration deformation.

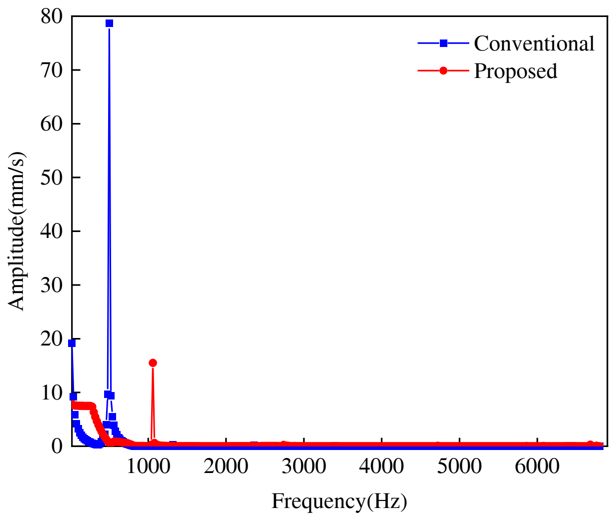

FIGURE 10. Vibration velocity.

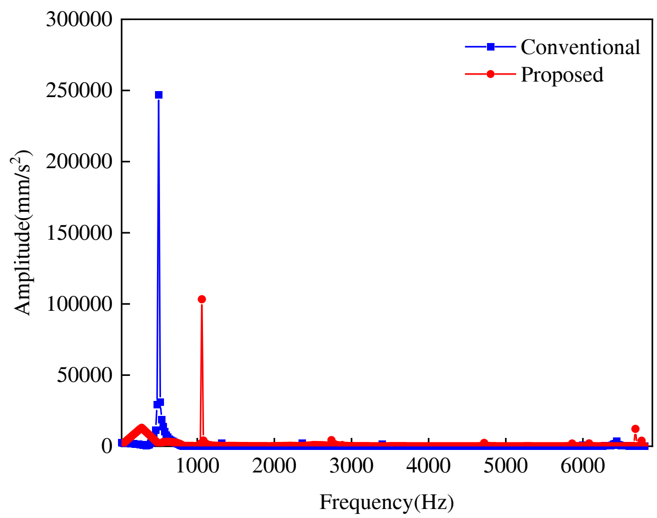

FIGURE 11. Vibration acceleration.

magnitudes are in the micrometer range. In these cases, the vibrations are not visually observable. However, a vibration displacement peak of 0.06 mm is recorded for the proposed machine. This value is reduced by 60% compared to the 0.15 mm of the conventional machine.

Vibration velocity and acceleration trends on the stator surface are consistent, as shown in Fig. 10 and Fig. 11. For the conventional machine, the maximum vibration velocity and acceleration are recorded at twice the fundamental frequency, reaching 78 mm/s and 247030 mm/s^2, respectively. In the proposed machine, auxiliary teeth are introduced to modify the magnetic permeability distribution. Higher-order electromagnetic force harmonics are thereby generated. Simultaneously, the symmetry of the magnetic field is altered by the alternate-pole structure. This modification excites the additional harmonic components. As a result, the peak vibration velocity and acceleration of the proposed machine are shifted to four times the fundamental frequency. Compared to the conventional machine, reductions of 80.12% in peak velocity and 58.19% in peak acceleration are achieved.

Figure 12 presents the acoustic noise distributions of the conventional and proposed machines. In Fig. 12(a), the conventional machine shows a maximum sound pressure level of 86.38dB, with extensive high-noise regions. In contrast, the proposed machine in Fig. 12(b) achieves a significantly reduced maximum sound pressure level of 62.31 dB, with a more uniform noise distribution and high-noise regions concentrated in localized areas. These results confirm the effectiveness of the proposed design in suppressing electromagnetic vibration and reducing acoustic noise radiation.

The above vibration analysis is performed under steady-state rated speed conditions. However, turbine input speed fluctuations are inevitable in hydropower applications and may affect the vibration behavior of the FRPMM. These fluctuations first modulate the frequencies of radial electromagnetic force harmonics via changes in the electrical frequency. When the shifted frequencies approach the natural frequencies of the sta-

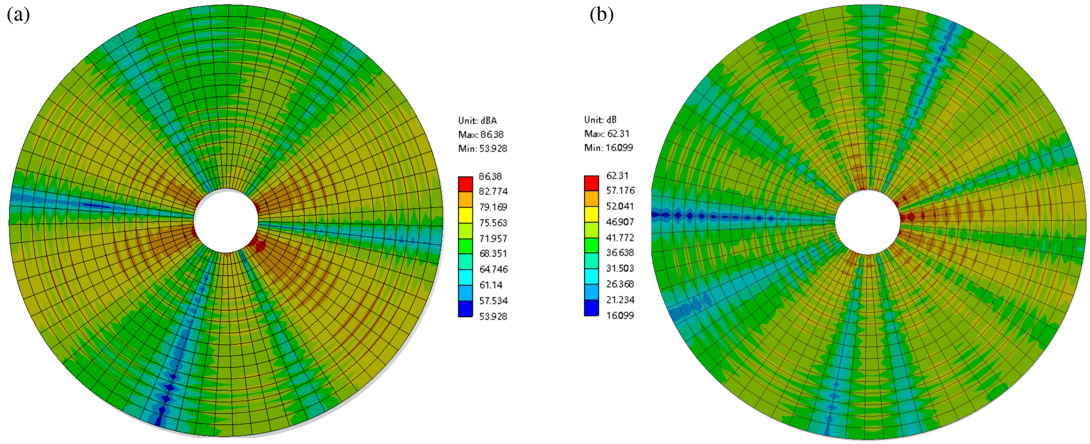

FIGURE 12. Acoustic noise. (a) Conventional machine and (b) the proposed machine.

tor structure, resonance-like vibration amplification may be induced. In addition, such variations may couple with the inherent torque ripple of the FRPMM through drivetrain dynamics, forming a potential positive feedback loop that further exacerbates the vibration response. Nevertheless, the actual impact of these coupling effects is highly application-dependent and requires further simulation analysis on a case-by-case basis.

6. CONCLUSION

This article studies effectiveness of a novel FRPMM for optimizing vibration characteristics. The MOGA is used to optimize radial force density, average torque, and torque ripple as optimization objectives to determine optimal structural parameters. The space-time distribution of the air-gap flux density and radial electromagnetic force is obtained by finite-element simulation. The modal analysis of the stator is carried out by Workbench to extract the machine's natural frequency. Parameters of vibration deformation, velocity, and acceleration are analyzed by harmonic response. The radial force density of FRPMM is reduced by 39.52% compared with that of the conventional machine, and the vibration is effectively suppressed.

The proposed PM chamfer relies on mature manufacturing processes. In small hydropower applications, larger machine dimensions lead to increased air-gap lengths, which provide greater design freedom. Moreover, since the chamfer only modifies the PM edge profile without altering its mounting or stress state, structural integrity is maintained, indicating promising engineering prospects.

Future work will examine the influence of turbine input speed fluctuations on vibration characteristics and carry out prototype fabrication and vibration testing to validate simulation results.

ACKNOWLEDGEMENT

This work was supported by the Science and Technology Project of Liujiaxia Hydropower Plant of State Grid Gansu Electric Power Company (Grant No. SG-GSLD00JJJS2600139).

REFERENCES

[1] Wei, L., T. Nakamura, and K. Imai, "Development and optimization of low-speed and high-efficiency permanent magnet generator for micro hydro-electrical generation system," *Renewable Energy*, Vol. 147, 1653–1662, 2020.

[2] Zhang, W., L. Dai, Z. Xiang, Q. Wu, S. Huang, and J. Gao, "Optimal design of hydro permanent magnet synchronous generators for improving annual cycle efficiency," *International Journal of Electrical Power & Energy Systems*, Vol. 131, 107096, 2021.

[3] Zhu, X., W. Hua, Z. Wu, W. Huang, H. Zhang, and M. Cheng, "Analytical approach for cogging torque reduction in flux-switching permanent magnet machines based on magnetomotive force-permeance model," *IEEE Transactions on Industrial Electronics*, Vol. 65, No. 3, 1965–1979, March 2018.

[4] Li, J., Y. Gao, C. Zhang, X. Zha, and R. Qu, "Pulsating torque suppression of flux reversal machines based on specific harmonic contributions of rotor permeance and PM MMF," *IEEE Transactions on Industry Applications*, Vol. 61, No. 5, 7129–7140, September 2025.

[5] Takiguchi, M., H. Sugimoto, N. Kurihara, and A. Chiba, "Acoustic noise and vibration reduction of SRM by elimination of third harmonic component in sum of radial forces," *IEEE Transactions on Energy Conversion*, Vol. 30, No. 3, 883–891, September 2015.

[6] Sun, T., J.-M. Kim, G.-H. Lee, J.-P. Hong, and M.-R. Choi, "Effect of pole and slot combination on noise and vibration in permanent magnet synchronous motor," *IEEE Transactions on Magnetics*, Vol. 47, No. 5, 1038–1041, May 2011.

[7] Li, B., Z. Yin, R. Cao, K. Wang, and Z. Wang, "Vibration and noise analysis and suppression of high torque density permanent magnet motor," in *2024 27th International Conference on Electrical Machines and Systems (ICEMS)*, 3640–3646, Fukuoka, Japan, November 2024.

[8] Wu, F., H. Liu, D. Li, J. Cao, Y. Wang, and C. Yang, "Vibration and noise optimization of surfaced mounted PMSM used in EMP," in *2025 IEEE International Conference on Mechatronics (ICM)*, 1–6, February 2025.

[9] Won, Y.-J., J.-H. Kim, S.-M. An, and M.-S. Lim, "Comparative study of cogging torque, torque ripple, and vibration on stator tooth chamfer types in permanent magnet synchronous motors," *IEEE Transactions on Magnetics*, Vol. 60, No. 9, 1–5, September 2024.

[10] Wang, X., D. Wang, C. Peng, B. Wang, and X. Wang, "Torsional vibration analysis and suppression of interior permanent magnet synchronous motor with staggered segmented rotor for electric vehicles," *IEEE Transactions on Transportation Electrification*, Vol. 10, No. 3, 6285–6294, September 2024.

[11] Yin, H., W. Hua, Z. Wu, and J. Du, "An efficient rotor-skewing model for mitigating electromagnetic vibration and noise in fractional-slot concentrated-winding permanent-magnet machines," *IEEE/ASME Transactions on Mechatronics*, Vol. 30, No. 2, 818–828, April 2025.

[12] Yuan, Y., Y. Wang, X. Li, Y. Chen, Y. Zheng, and R. Qu, "Analysis and suppression of synchronous reluctance motors with mirror asymmetric rotors," in *2024 27th International Conference on Electrical Machines and Systems (ICEMS)*, 3593–3597, November 2024.

[13] Peng, C., D. Wang, Z. Feng, and B. Wang, "A new segmented rotor to mitigate torque ripple and electromagnetic vibration of interior permanent magnet machine," *IEEE Transactions on Industrial Electronics*, Vol. 69, No. 2, 1367–1377, February 2022.

[14] Hua, W. and X. Zhu, "Overview of flux-reversal permanent magnet machine and its key technologies," *Proceedings of the CSEE*, No. 8, 2657–2669, 2020.

[15] Zhu, S., W. Zhao, J. Ji, G. Liu, and C. H. T. Lee, "Generation mechanism and suppression measure of electromagnetic vibration in permanent magnet synchronous machine: A review," *IEEE Transactions on Transportation Electrification*, Vol. 10, No. 4, 9513–9528, December 2024.

[16] Shah, S. H., Y.-C. Wang, D. Shi, and J.-X. Shen, "Analysis of radial force, vibration, and noise in low-speed, high-torque density spoke-type PMSMs with symmetric and asymmetric assisted poles designs," *CES Transactions on Electrical Machines and Systems*, Vol. 9, No. 1, 15–25, March 2025.

[17] Cai, Y., F. S. El-Faouri, A. Chiba, and S. Yoshizaki, "Magnetostriction effect on vibration and acoustic noise in permanent magnet synchronous motors," *IEEE Open Journal of Industry Applications*, Vol. 5, 442–454, 2024.

[18] Jansen, J. and A. Mertens, "Compensation of radial mode 0 vibration of an electrically excited synchronous machine using harmonic field current injection," in *2024 27th International Conference on Electrical Machines and Systems (ICEMS)*, 1359–1363, Fukuoka, Japan, November 2024.

[19] Liu, F., J. Liu, and Y. Yang, "An optimization design for reducing cogging torque in permanent magnet synchronous motors," in *2024 27th International Conference on Electrical Machines and Systems (ICEMS)*, 156–161, Fukuoka, Japan, November 2024.

[20] Zhou, Y., X. Wei, L. Yan, and X. He, "Hybrid analytical-numerical electromagnetic vibration calculation method for surface-inserted PMSMs with skewed slots," *IEEE Transactions on Energy Conversion*, Vol. 39, No. 4, 2654–2663, December 2024.

[21] Jing, L., W. Liu, W. Tang, and R. Qu, "Design and optimization of coaxial magnetic gear with double-layer PMs and spoke structure for tidal power generation," *IEEE/ASME Transactions on Mechatronics*, Vol. 28, No. 6, 3263–3271, December 2023.

[22] Wang, Y., Z.-Q. Zhu, J. Feng, S. Guo, Y. Li, and Y. Wang, "Investigation of unbalanced magnetic force in fractional-slot permanent magnet machines having an odd number of stator slots," *IEEE Transactions on Energy Conversion*, Vol. 35, No. 4, 1954–1963, December 2020.

[23] Min, Z., L. Jing, T. Wang, and R. Qu, "A partitioned stator flux switching PM machine with strongly coupled flux reversal effect," *IEEE Transactions on Transportation Electrification*, 1–1, 2026.